



PAPER • OPEN ACCESS

A microphysiological model of bone development and regeneration

To cite this article: Ian T Whelan *et al* 2023 *Biofabrication* **15** 034103

View the [article online](#) for updates and enhancements.

You may also like

- [Effect of different level of urea addition for rice straw fermentation application: *in vitro* evaluation](#)
Firsoni, Nurdia Ekani and Teguh Wahyono
- [Prolonged *in vitro* precultivation alleviates post-implantation inflammation and promotes stable subcutaneous cartilage formation in a goat model](#)
Yi Liu, Dan Li, Zongqi Yin et al.
- [In vitro study of the antioxidant activity of extracts from dried biomass of callus, cell suspension, and root cultures](#)
O O Babich, L N Skrypnik and A V Pungin

Biofabrication



PAPER

OPEN ACCESS

RECEIVED
1 August 2022

REVISED
3 May 2023

ACCEPTED FOR PUBLICATION
18 May 2023




PUBLISHED
6 June 2023

Original content from this work may be used under the terms of the [Creative Commons Attribution 4.0 licence](https://creativecommons.org/licenses/by/4.0/).

Any further distribution of this work must maintain attribution to the author(s) and the title of the work, journal citation and DOI.



A microphysiological model of bone development and regeneration

Ian T Whelan^{1,4} , Ross Burdis¹, Somayah Shahreza⁵, Emad Moeendarbary^{5,6,7}, David A Hoey^{1,2,3,4}  and Daniel J Kelly^{1,2,3,4,*} 

¹ Trinity Centre for Biomedical Engineering, Trinity Biomedical Sciences Institute, Trinity College Dublin, Dublin, Ireland

² Advanced Materials and Bioengineering Research Centre (AMBER), Royal College of Surgeons in Ireland and Trinity College Dublin, Dublin, Ireland

³ Department of Mechanical, Manufacturing and Biomedical Engineering, School of Engineering, Trinity College Dublin, Dublin, Ireland

⁴ CURAM Center for Research in Medical Devices, National University of Ireland, Galway, Ireland

⁵ Department of Mechanical Engineering, University College London, London, United Kingdom

⁶ Department of Biological Engineering, Massachusetts Institute of Technology, Cambridge, United States of America

⁷ 199 Biotechnologies Ltd, Gloucester Road, W2 6LD London, United Kingdom

* Author to whom any correspondence should be addressed.

E-mail: kellyd9@tcd.ie

Keywords: development, microphysiological, model, bone, organ on chip

Supplementary material for this article is available [online](#)

Abstract

Endochondral ossification (EO) is an essential biological process that underpins how human bones develop, grow, and heal in the event of a fracture. So much is unknown about this process, thus clinical manifestations of dysregulated EO cannot be adequately treated. This can be partially attributed to the absence of predictive *in vitro* models of musculoskeletal tissue development and healing, which are integral to the development and preclinical evaluation of novel therapeutics. Microphysiological systems, or organ-on-chip devices, are advanced *in vitro* models designed for improved biological relevance compared to traditional *in vitro* culture models. Here we develop a microphysiological model of vascular invasion into developing/regenerating bone, thereby mimicking the process of EO. This is achieved by integrating endothelial cells and organoids mimicking different stages of endochondral bone development within a microfluidic chip. This microphysiological model is able to recreate key events in EO, such as the changing angiogenic profile of a maturing cartilage analogue, and vascular induced expression of the pluripotent transcription factors SOX2 and OCT4 in the cartilage analogue. This system represents an advanced *in vitro* platform to further EO research, and may also serve as a modular unit to monitor drug responses on such processes as part of a multi-organ system.

1. Introduction

Endochondral ossification (EO) is a process critical to the development, post-natal growth and healing of the long bones of the human skeleton. During EO a cartilage template matures to hypertrophy, initiating a pro-angiogenic program resulting in vascular invasion that is integral to the transformation of cartilage into bone [1, 2]. The specifics of how bone develops in this way, and specifically how vasculature initiates the cartilage to bone transformation is still not fully understood. A deeper understanding of EO will bring about not just an improved basic understanding

of this key aspect of bone biology, but could also lead to improvements in the treatment of a number of skeletal diseases, such as fracture non-unions [3], chondrodysplasias [4], and osteochondrosis [5]. Furthermore, such developments may improve our understanding of conditions involving aberrant cartilage to bone transformation, such as osteoarthritis [6], as well as enabling the development of novel tissue engineering strategies for the treatment of large bone defects [7]. At present, autografting is the current gold standard approach for large bone defect repair, but has inherent drawbacks such as donor site morbidity and limited supply [8]. As EO is central to

long bone development and secondary fracture healing, recapitulating this process is forming the basis to emerging alternative tissue engineering strategies to repair large bone defects [9, 10]. Such approaches involve the implantation of a pre-cultured cartilaginous or hypertrophic tissue to stimulate the healing process and drive regeneration [11], and has shown significant promise in preclinical studies [10, 12].

Rodent models are currently the primary method for studying EO in both developmental [13] and regenerative contexts such as fracture healing [1]. These animal models are essential for research, as no *in vitro* system can replicate the complexity of an entire organism. However, rodents do not present haversian remodelling or closure of the epiphyseal growth plate as occurs in humans [14, 15], and therefore the underlying mechanisms of EO may differ between the species. Alternatively, *in vitro* models are less expensive, potentially of human origin, and can produce more specific, higher resolution information than animal models. A number of *in vitro* systems exist to model EO; for example, the murine-derived ATDC-5 cell line can undergo cellular condensation, proteoglycan synthesis, collagen type II secretion [16], and hypertrophic mineralisation [17, 18], and have been used as model cells for EO research. Additionally, *ex vivo* mesenchymal micromass cultures from the developing limb bud [19], isolated chondrocytes [20] and growth cartilage explants [21] can be used for EO research. The drawback of these models is that they are typically not of human origin, which in itself can result in poor predictive ability [22]. Additionally, these systems lie on either end of a spectrum of *in vitro* biological complexity; exhibiting a substantial trade off in experimental control and physiological relevance.

Next generation *in vitro* models of EO should exist in the centre of this spectrum, incorporating more physiological relevance to facilitate the advanced study of key developmental and regenerative processes. 3D bioprinting technologies, for example, can be used to generate such model tissues and have been employed to fabricate vascularised osseous tissues *in vitro* [23, 24]. Additionally, 3D bioprinting has been used to engineer constructs capable of executing a developmental paradigm to promote endochondral bone formation *in vivo* [25]. Alternatively, microphysiological systems (MPSs) are a candidate platform on which these next generation models can be built. A key feature of MPS technology relevant to modelling EO is the ability to generate three-dimensional tissues with physiologically relevant perfusable vasculature [26], which, if incorporated into an *in vitro* model of EO, could facilitate probing the essential role of vasculature in directing the transition of a cartilage template into bone, a crucial phase of EO. MPS technology has been used extensively to study vasculature [27], and its role in specific disease processes such as metastasis [28]. However, MPS

applications in musculoskeletal research, particularly in cartilage and bone, are only beginning to emerge [29, 30]. Thus, MPS technology is particularly suitable for building models of cartilage biology that are more physiologically relevant.

The aim of this paper is to develop and validate a MPS model of EO. More specifically, the aim is to develop a MPS to model the vascular invasion of cartilage during EO in developing (or regenerating) bone. Thus, to further understand this developing bone–vasculature crosstalk, microscale developing bone organoids (μ DBO) that represent different stages along the endochondral pathway were vascularised in an MPS device, and their response to vascularisation at the gene and tissue level was characterised. This MPS is able to predict the changing angiogenic profile of maturing cartilage, as well as the vascular induced activation of pluripotency associated genes in chondrocytes during EO.

2. Methods

2.1. Cell culture

2.1.1. Media formulations

2.1.1.1. Expansion medium (XPAN)

XPAN medium was used for monolayer expansion. XPAN medium consisted of high-glucose GlutaMAX Dulbecco's modified Eagle's medium (DMEM) supplemented with 10% v/v fetal bovine serum, 100 U ml⁻¹ penicillin, 100 mg ml⁻¹ streptomycin (all Gibco Biosciences, Dublin, Ireland) and 5 ng ml⁻¹ FGF-2 (Peprotech, UK).

2.1.1.2. Basic chemically defined medium (CDM–)

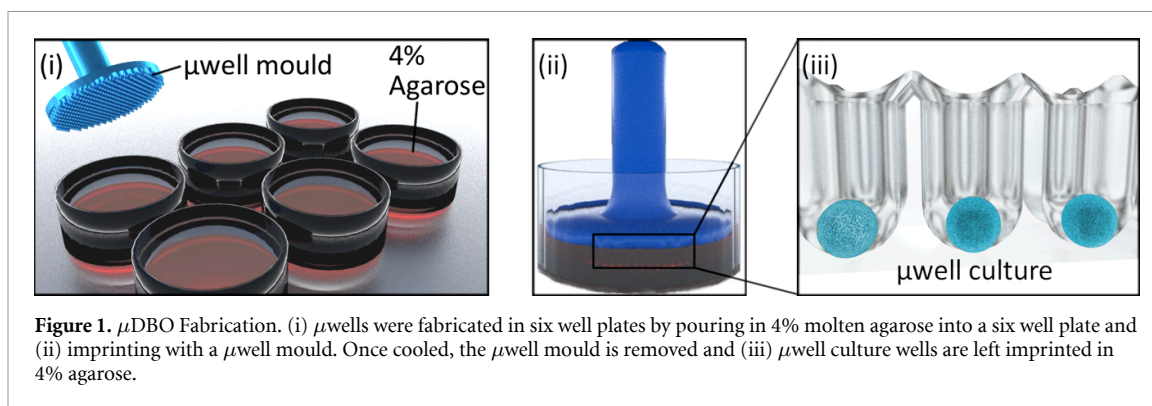
CDM– medium was used for undifferentiated (UD) μ DBO μ well culture. Chemically defined medium was prepared by adding 100 U ml⁻¹ penicillin, 100 mg ml⁻¹ streptomycin (all Gibco Biosciences, Dublin, Ireland), 100 μ g ml⁻¹ sodium pyruvate, 40 μ g ml⁻¹, L-proline, 50 μ g ml⁻¹ and 1.5 mg ml⁻¹ bovine serum albumin (Sigma Aldrich, Ireland) to DMEM.

2.1.1.3. Fully supplemented chemically defined medium (CDM \pm)

CDM+ medium was used for early cartilage (EC) and mature cartilage (MC) μ DBO μ well culture. CDM– was supplemented with; 4.7 μ g ml⁻¹ L-ascorbic acid-2-phosphate, 4.7 μ g ml⁻¹ linoleic acid, 10 mg ml⁻¹ insulin, 5.5 mg ml⁻¹ transferrin, 6.7 μ g ml⁻¹ selenium (Gibco), 100 nM dexamethasone (Sigma-Aldrich, Ireland), and 10 ng ml⁻¹ of human transforming growth factor-b3 (TGF-b3) (Peprotech, UK).

2.1.1.4. Hypertrophic medium (HYP)

HYP was used for hypertrophic cartilage (HC) μ well culture, CDM– was supplemented with 4.7 μ g ml⁻¹ L-ascorbic acid-2-phosphate, linoleic



acid, 10 mg ml⁻¹ insulin, 5.5 mg ml⁻¹ transferrin, 6.7 μ g ml⁻¹ selenium (Gibco), 100 nM dexamethasone (Sigma–Aldrich, Ireland), 7.5 mM β -glycerophosphate, and 25 ng ml⁻¹ L-Thyroxine (Sigma Aldrich, Ireland).

2.1.1.5. Endothelial growth medium–2Microvascular (EGM)

EGM-2MV (herein referred to as EGM) was used for human umbilical vein endothelial cells (HUVECs) expansion and MPS culture. Endothelial Basal Media (CC-3156, Lonza) was fully supplemented (CC-4147) as per the manufacturer's instructions.

2.1.2. Cell culture and expansion

2.1.2.1. Human bone marrow stromal cells (hBMSCs)

Whole human bone marrow (Lonza, USA) was purchased and hBMSCs were isolated. Whole bone marrow was plated at 2000 cells cm⁻² and expanded in XPAN for one week at 37 °C, 5% O₂ and 5% CO₂. Once colonies had formed, cells were trypsinized and subcultured until sufficient cell numbers were achieved, cells were then frozen down and stored in liquid nitrogen (LN₂) before use. The donor used was evaluated for osteogenic, adipogenic, and chondrogenic capacity. For experimental expansion, hBMSCs were plated at 5000 cells cm⁻², expanded in XPAN until confluent and passaged at 80% confluence. hBMSCs at P4 were used for all experiments.

2.1.2.2. HUVECs

Green fluorescent protein expressing HUVECs, herein referred to as HUVECs, were purchased from Angio-proteomie. HUVECs were expanded in microvascular endothelial growth media (EGM-2MV, Lonza) on rat-tail collagen coated T75 flasks at 10 μ g cm⁻². HUVECs were used at passage 8 for all experiments.

2.1.2.3. μ DBO formation and harvesting

μ DBOs were formed by seeding hBMSCs on an a 401 μ well agarose mould [31]. Custom designed master stamps were 3D printed (Form 3, Formlabs, USA), and sterilised with ethylene oxide before moulding.

To create the multiwell moulds, 3 ml of 4% molten agarose (Sigma, Ireland) was pipetted into each well of a six well plate, stamps inserted, and agarose allowed to cool (figure 1). Upon removal of stamps, 3 ml of media is added and exchanged daily for two days to allow media contents to equilibrate in the agarose.

To form μ DBOs, hBMSCs were pipetted on to the agarose mould, allowed to settle for 30 min in an incubator and centrifuged at 700 g for 5 min. About 3 ml of media was then exchanged every other day for the duration of culture. Four different organoids were fabricated to represent increasing cartilage tissue maturity: UD μ DBOs (-ve control) were cultured in CDM– at 5% O₂ for 7 days, EC μ DBOs were cultured in CDM+ at 5% O₂ for 7 days, MC μ DBOs were cultured in CDM+ at 5% O₂ for 21 days, and HC μ DBOs were cultured for 21 days in CDM+ at 5% O₂ and a further 7 days in HYP media at 20% O₂.

To harvest μ DBOs, high media flow from a 20 ml syringe and 20 g needle was used to release μ DBOs from each individual well. Suspended μ DBOs were then harvested directly from the medium, while μ DBOs remaining in the well were removed by flipping the agarose moulds into a fresh six well plate and centrifuging for 600 g for 5 min and collecting in media. μ DBOs were passed through a 500 μ m filter to remove fused μ DBOs and agarose fragments.

2.1.3. μ DBO diameter

μ DBO diameter was determined using image analysis. Images of μ DBOs were taken during culture with a brightfield microscope and images were measured manually using FIJI software [32].

2.1.4. Biochemical analysis

After μ well culture, μ DBOs were washed in phosphate buffered saline (PBS) and frozen in liquid nitrogen and stored at –80 °C. Each construct was digested with papain (125 μ g ml⁻¹) in 0.1 M sodium acetate, 5 mM L-cysteine–HCL, 0.05 M ethylenediaminetetraacetic acid, pH 6.0 (all from Sigma–Aldrich) at 60 °C and 10 rpm for 18 h. DNA content was quantified using a Quant-iT™ PicoGreen™ dsDNA Assay Kit (Invitrogen) as per the manufacturer's

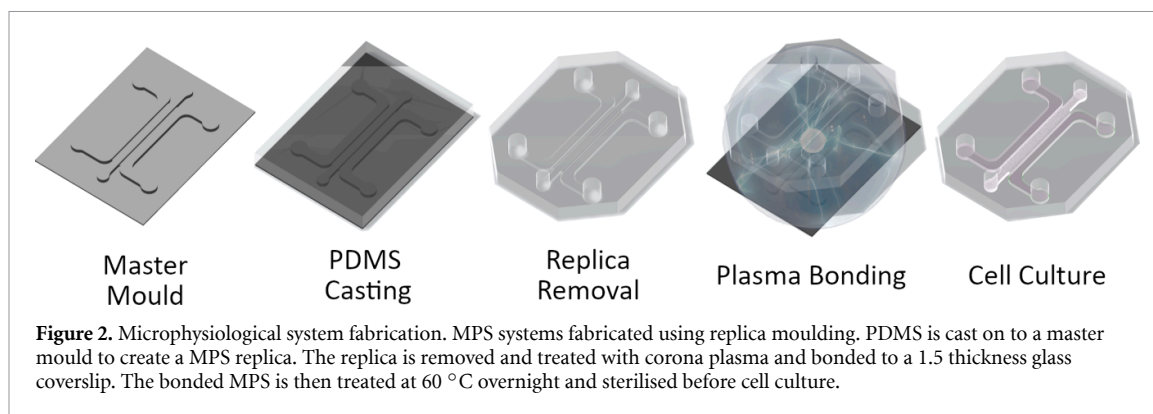


Figure 2. Microphysiological system fabrication. MPS systems fabricated using replica moulding. PDMS is cast on to a master mould to create a MPS replica. The replica is removed and treated with corona plasma and bonded to a 1.5 thickness glass coverslip. The bonded MPS is then treated at 60 °C overnight and sterilised before cell culture.

instructions. Sulphated glycosaminoglycans (sGAGs) were quantified using a 1,9-dimethyl-methylene blue (DMMB) assay. Briefly, digested samples were mixed with a DMMB staining solution and absorbance was measured at 530 nm and 590 nm. sGAG levels were interpolated from a standard curve of 530/590 nm absorbance ratio using a chondroitin sulfate standard.

2.1.5. Live-dead assay

Cell viability was assessed after μ well culture using a LIVE/DEAD™ viability/cytotoxicity assay kit (Invitrogen, Bioscience, Ireland). μ DBOs were washed with PBS followed by incubation with PBS containing 2 μ M calcein AM (green fluorescence of membrane for live cells) and 4 μ M ethidium homodimer-1 (red fluorescence of DNA for dead cells; both from Cambridge Bioscience, UK). μ DBOs were again washed in PBS, imaged with a Leica SP8 scanning confocal excited at 494 nm and 528 nm, and read at 517 nm and 617 nm respectively.

2.1.6. Microphysiological chip fabrication

Microfluidic devices were fabricated using replica moulding (figure 2). Master moulds were fabricated by laser cutting the channel geometries from 1 mm thick PMMA Poly(methyl methacrylate) sheets and adhering to 30 mm diameter PMMA plates using acrylic glue (Scigrup 4SC, USA). Master moulds were then glued to the bottom of 100 mm diameter petri dishes. To create microfluidic chips, sylgard 184 polydimethylsiloxane (Dowsil, USA), was mixed at 10:1 (polymer:catalyst), degassed under 40 mbar vacuum for 10 min and poured on master moulds. PDMS was allowed to cure overnight at 80 °C. Once cured, PDMS replicas were removed by cutting around the circumference of the mould and removing with a spatula. PDMS replicas were then trimmed and cleaned using adhesive tape. To form the microfluidic devices, PDMS replicas and 1.5 thickness glass coverslips were plasma treated with corona plasma (Corona SB, BlackHole Labs, Paris) for 1 min each and pressed together. Devices were then placed in an oven overnight at 60 °C for hydrophobic recovery. Finally, devices were sterilised using

ethylene oxide and allowed to air for two days before culture.

2.1.7. Microfluidic device culture

Microfluidic devices were seeded with a co-culture of μ DBOs and HUVECs. Each device holds 100 μ l of hydrogel. μ DBOs and HUVECs were harvested and resuspended in medium containing with 4 U ml⁻¹ thrombin (Sigma Aldrich, Ireland). About 50 μ l of cell/ μ DBO suspension was then mixed with an equal volume of 6 mg ml⁻¹ bovine fibrinogen (Sigma Aldrich, Ireland), mixed and quickly pipetted into the microfluidic devices to minimise μ DBO settling. Fibrin was allowed to clot for 40 min in a humidified incubator, after which EGM-2MV is added to each device. Media was exchanged daily. Final concentrations were 2000 μ DBOs ml⁻¹ (200/device) and 4×10^6 HUVECs/ml (400 000/device).

2.1.8. Histology

μ well culture μ DBOs were fixed overnight at 4 °C in 4% paraformaldehyde (PFA), washed with PBS and allowed to settle at the bottom of a well of a flat bottom 96 well plate. Once settled, PBS was removed, and a 4% molten agarose solution was pipetted on to the settled μ DBOs and allowed to cool to hold them in place. For MPS culture, devices were washed with PBS, fixed with 4% PFA at 4 °C overnight, and again washed with PBS. To remove tissues from the MPS devices, coverslips were covered with tape to avoid cracking and a scalpel was used to separate the PDMS device from the coverslip. Both μ well culture and MPS samples were then dehydrated in a graded series of ethanol, embedded in paraffin wax, sectioned at 5 μ m and affixed to microscope slides. Samples were stained with H + E to assess cell and tissue morphology, picrosirius red to assess collagen deposition, alizarin red to assess mineralisation, and alcian blue to assess glycosaminoglycan (GAG) deposition.

2.1.9. Vascular network morphology analysis

Entire MPS devices were imaged after seven days to analyse vascular formation. Images were analysed using a custom macro to automate processing in FIJI [32]. Two regions of interest were cropped for

the analysis; vasculature formation in the bulk gel, and vasculature formation around the μ DBO. The images of these vasculature regions were processed for improved signal to noise ratio; images were despeckled, contrast adjusted and Gaussian blurred and thresholded to form a binary image. Finally this image was processed to form a simple skeletonised image and analysed using FIJI's analyse skeleton function [33]. Automated thresholding was checked against the original image. To compare vascularisation in the two regions, a $1.37 \mu\text{m}^2$ area was analysed. For regions without μ DBOs, this region is a simple square of area $1.37 \mu\text{m}^2$. For regions with a μ DBO, this region is a square with the area of the μ DBO removed from the analysis, but also of area $1.37 \mu\text{m}^2$ (supplementary figure 1).

2.1.10. Perfusion

Vascular network perfusion was evaluated at day 7 by perfusion of fluorescent dextran. 70 kDa rhodamine conjugated dextran (Sigma Aldrich, Ireland) was diluted in PBS to 2 mg ml^{-1} , vortexed and stored at 4°C protected from light. To perfuse the vascular networks contained in the MPS devices, media was removed from both media side channels and device placed on a Leica SP8 scanning confocal microscope stage. Once positioned for imaging, dextran was introduced to one side of the vascular network by filling the channel to the top of the feeding port of each device; creating a hydrostatic pressure gradient across the vascular network. Images were taken immediately to avoid excessive diffusion of dye across the bulk hydrogel.

2.1.11. Gene expression analysis

2.1.11.1. Sample handling

At termination of μ DBO μ well culture, μ DBOs were washed in PBS and snap frozen in liquid nitrogen before RNA isolation. Upon termination of in MPS culture, fibrin gels containing the μ DBO/HUVEC co-culture was removed from the MPS device. The hydrogel was then transferred to 1.5 ml Eppendorf and 1 ml of a fibrinolytic solution; prepared by dissolving 50 FU ml^{-1} (fibrin degradation units) of nattokinase (NSK-SD; Japan Bio Science Laboratory Co. Ltd), was added and rotated at 37° for 40 min. The resulting μ DBO/HUVEC suspension was passed through a $100 \mu\text{m}$ cell strainer and washed with 10 ml of PBS to separate μ DBOs from individual HUVECs. The μ DBOs were then retrieved from the filter, placed in a 1.5 ml Eppendorf, spun down to remove excess PBS and frozen in liquid nitrogen. Samples were stored at -80°C until RNA isolation.

2.1.11.2. RNA isolation and cDNA transcription

μ DBOs frozen at -80°C were thawed on ice. Once thawed, $500 \mu\text{l}$ of TRIzol (Invitrogen, LifeTechnologies, Carlsbad, CA) was added and μ DBOs were mechanically disrupted with a pestle

(treated with diethyl pyrocarbonate) for 10 s and centrifugation to pull insoluble material to the bottom of the Eppendorf. This process of disruption and centrifugation was repeated until no insoluble material remained in the Eppendorf (~ 2 times). The pestle was then rinsed with another $500 \mu\text{l}$ of TRIzol into the sample for a total volume of 1 ml. The sample was then left to stand at room temperature for 7 min. About $200 \mu\text{l}$ Chloroform (Sigma, Ireland), was then added to each sample, vortexed and incubated for 5 min at 4°C . Samples were then centrifuged at $12\,000 \text{ g}$ for 15 min at 4°C . About $500 \mu\text{l}$ of the top aqueous, RNA containing phase of the sample was removed and transferred into an RNase free Eppendorf. About $500 \mu\text{l}$ of 2-Propanol (Sigma, Ireland) and $2 \mu\text{l}$ of GlycoBlue co-precipitant (Invitrogen) were mixed to precipitate the RNA and left to stand at room temperature for 10 min. Samples were then centrifuged at $14\,000 \text{ g}$ for 15 min at 4°C . Supernatants were removed and each RNA pellet was washed with 1 ml of 75% ethanol and incubated at -20°C for one day. Samples were then centrifuged at $7\,000 \text{ g}$ for 5 min at 4°C . All ethanol was then removed and the RNA pellet was resuspended in $20 \mu\text{l}$ of RNase free water. RNA quantity and quality was checked with a spectrophotometer.

RNA samples were immediately transcribed into cDNA following isolation. Reverse transcription was carried using a cDNA RT kit (Applied Biosystems, USA) according to the manufacturer's instructions using a thermocycler. Following reverse transcription, cDNA was measured using a QubitTM ssDNA assay kit (Invitrogen, USA) as per the manufacturer's instructions using a QubitTM fluorometer (Invitrogen, USA). Samples were stored at a concentration of $2 \text{ ng}/\mu\text{L}$ at -20°C .

2.1.11.3. PCR

Levels of gene expression were measured with real-time PCR (ABI 7500-fast, Applied Biosystems) using SYBR green master mix (Applied Biosystems) and human specific primers (table 1). The quantity of gene transcripts was normalised to that of a stable housekeeping gene, in this case GAPDH. Efficiency of all primer pairs were calculated by 10-fold serial dilutions of cDNA starting at 50 ng per reaction.

2.1.12. Statistical analysis

GraphPad Prism (GraphPad, USA) was used for all statistical analysis. Comparisons made between two groups, or multiple groups were conducted using student's *t*-test or one-way analysis of variance (ANOVA) respectively. Two-way ANOVA was used to compare multiple groups at multiple levels. Non-parametric tests were used where assumptions of normality could not be justified. Graph notation for deemed significance is as follows: * $p < 0.05$, ** $p < 0.01$, *** $p < 0.001$, **** $p < 0.0001$.

Table 1. List of primer pairs used for PCR reactions.

Gene name	Gene full name	Forward/Reverse	T _m (°C) in use	T _m (°C) predicted
GAPDH	Glyceraldehyde-3-Phosphate Dehydrogenase	F: 5' ACAGTTGCCATGTAGACC 3' R: 5' TTGAGCACAGGGTACTTTA 3'	60	59.0 58.3
RUNX2	Runt-Related Transcription Factor 2	F: 5' GCAGTATTTACAACAGAGGG 3' R: 5' TCCCAAAAGAAGTTTGTCTG 3'	60	58.1 59.3
MMP-13	Matrix Metalloproteinase 13	F: 5' AGGCTACAACCTGTTTCTTG 3' R: 5' AGGTGTAGATAGGAAACAT 3'	60	58.4 55.1
COL10a1	Collagen Type X Alpha 1 Chain	F: 5' GCTAGTATCCTTGAACCTGG 3' R: 5' CCTTACTCTTTATGGTGTA 3'	60	50.2 54.5
SOX2	SRY-Box Transcription Factor 2	F: 5' ATAATAACAATCATCGGCGG 3' R: 5' AAAAAGAGAGAGGCAAAC 3'	60	57.1 58.1
POU5F1 (OCT4)	POU Class 5 Homeobox 1	F: 5' GATCACCTGGGATATACAC 3' R: 5' GCTTGCATATCTCCTGAAG 3'	60	58.1 59.1
NANOG	Nanog Homeobox	F: 5' CCAGAACCAGAGAATGAAATC 3' R: 5' TGGTGGTAGGAAGAGTAAAG 3'	60	60.1 55.9
THBS1	Thrombospondin 1	F: 5' GTGACTGAAGAGAACAAAGAG 3' R: 5' CAGCTATCAACAGTCCATTC 3'	60	55.6 57.3
SPARC	Secreted Protein Acidic and Cysteine Rich	F: 5' AGTATGTGTAACAGGAGGAC 3' R: 5' AATGTGCTAGTGTGATTGG 3'	60	52.9 57.6
COL18a1	Collagen Type XVIII Alpha 1 Chain	F: 5' TTACGACAGCAATGTGTTTG 3' R: 5' AGAAAGTCAAACGGAAACTG 3'	60	59.8 58.4

3. Results

3.1. Fabrication of DBOs for modelling EO

To investigate the changing cross-talk between vasculature and developing bone as it matures, microscale cellular analogues of developing bone (here termed μ DBOs) suitable for MPS applications were utilised. hBMSCs were aggregated in a μ well culture system prior to seeding in vascularised MPS devices. These μ DBOs can be maintained in culture until they progress towards an HC phenotype and accumulate a mineralised cartilage matrix, or removed from culture at earlier timepoints for DBOs representative of earlier stages of maturation (figures 3(A) and (B)). GAG deposition (normalised to DNA) increases as μ DBOs mature, with no further increase as they progress from MC to HC (figure 3(C)). Cell and tissue distribution throughout the μ DBOs was also analysed using a hematoxylin and eosin stain. Nuclei and extracellular matrix were observed throughout the engineered tissues (figure 3(D)). Finally, gene expression analysis revealed a culture duration dependent expression of genes associated with hypertrophy and osteogenesis; with the relative expression of *RUNX2*, *MMP13* and *COL10a1* increasing in the DBOs as they mature from EC, to MC and finally to HC (figure 3(E)).

3.2. Vascularisation of DBOs in a MPS device

Having developed μ DBOs to model developing endochondral bone, these organoids were then vascularised within a MPS device (figure 4(A)). To this end, HUVECs and MC μ DBOs were seeded into MPS devices within a fibrin hydrogel, resulting in the development of vascular networks around the μ DBOs

over seven days in culture. In order to optimise resource requirements for the model, two μ DBOs cell densities, 4000 cells/ μ DBO (as per previous figure) and 1000 cells/ μ DBO were evaluated. Additionally, to better mimic the low oxygen environment in a fracture callus, and given the sensitivity of osteoprogenitors to oxygen tension [34], 20% O₂ and 5% O₂ levels were also investigated. 4000 cell μ DBOs cells are viable (figure 4(B)), whereas in 1000 cell μ DBOs some cell death is observed, and disconnected vasculature forms with evidence of cell debris, which was confirmed semi quantitatively (figure 4(D)). Furthermore, 4000 cell μ DBOs also supported the development of perfusable vasculature within 75% of MPS devices, as evident by the transport of 70kDa rhodamine conjugated dextran through the vascular networks at 20% O₂. (figure 4(C)). At lower levels of external oxygen (5% O₂), the μ DBO were viable and vascular network formation was observed, however these networks were not perfusable. Given the favourable network formation and perfusion characteristics of the 4000 cells/ μ DBO group at 20% O₂, these experimental parameters were used in subsequent studies.

3.3. Vascular network development is dependent on the phenotype of the DBOs

Having identified conditions to vascularise the μ DBOs within the MPS device, the next step was to characterise μ DBO-vascular cross talk and assess whether the phenotype of the μ DBOs (EC, MC, HC) influenced the development of the vascular network. At day 3 of MPS culture, no discernible differences were observable between groups, as vascular structures have not formed and cross talk between the two

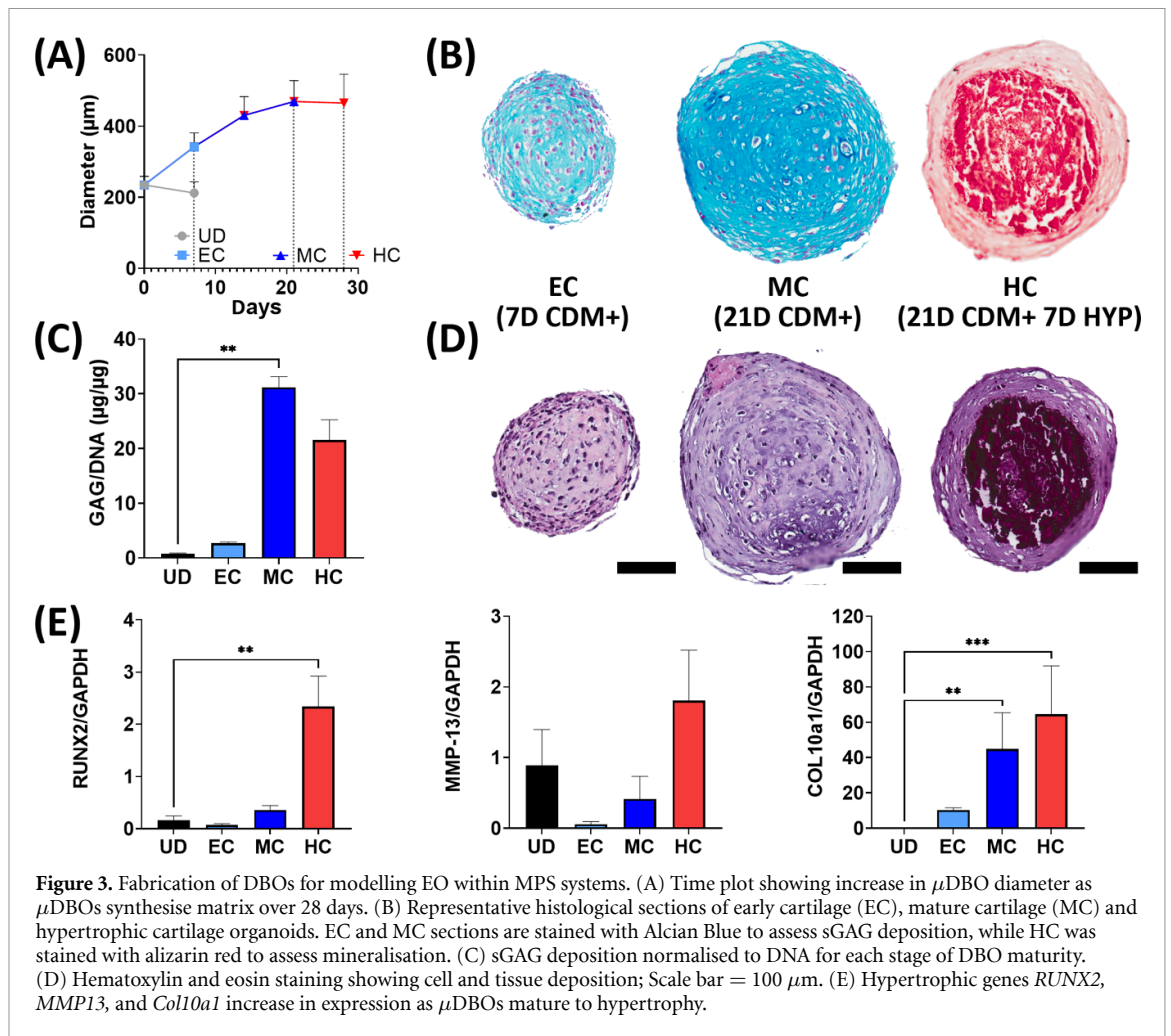
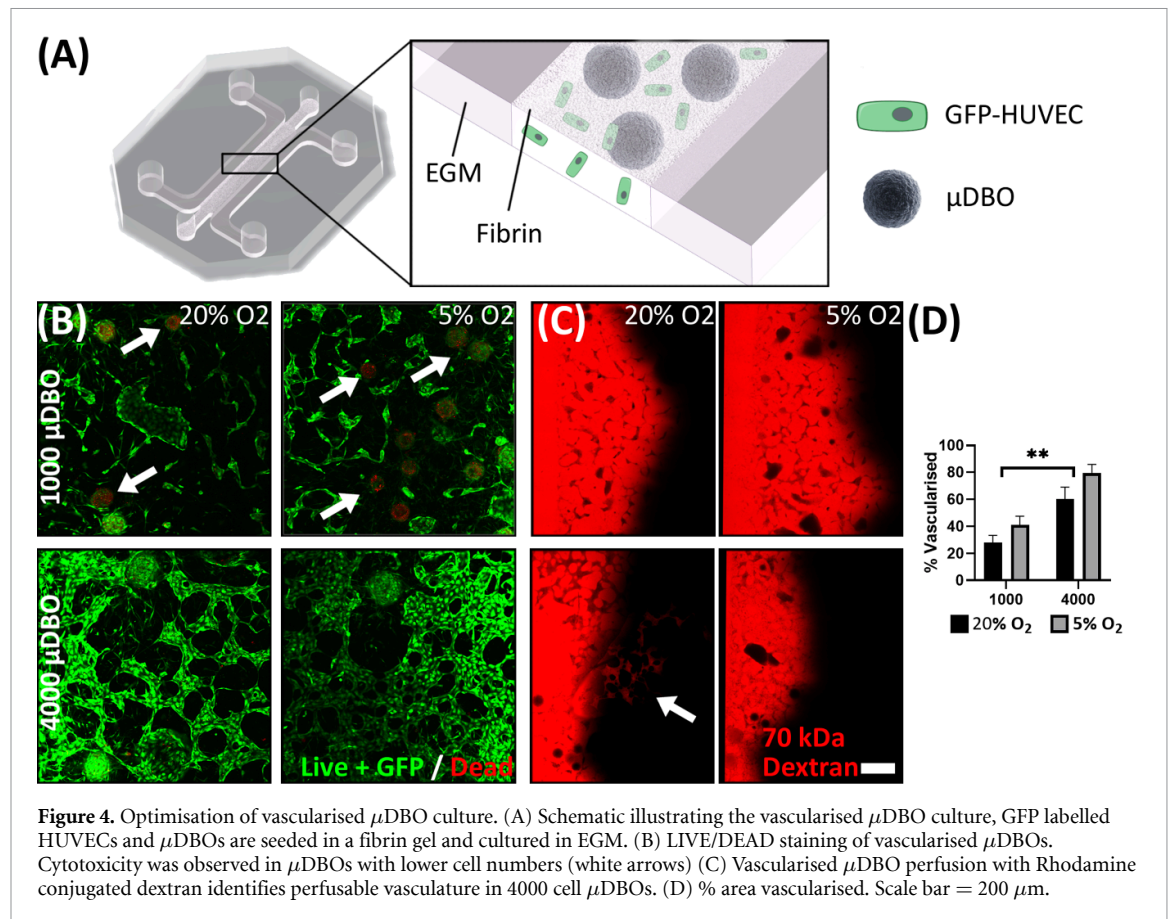


Figure 3. Fabrication of DBOs for modelling EO within MPS systems. (A) Time plot showing increase in μ DBO diameter as μ DBOs synthesise matrix over 28 days. (B) Representative histological sections of early cartilage (EC), mature cartilage (MC) and hypertrophic cartilage organoids. EC and MC sections are stained with Alcian Blue to assess sGAG deposition, while HC was stained with alizarin red to assess mineralisation. (C) sGAG deposition normalised to DNA for each stage of DBO maturity. (D) Hematoxylin and eosin staining showing cell and tissue deposition; Scale bar = 100 μ m. (E) Hypertrophic genes *RUNX2*, *MMP13*, and *Col10a1* increase in expression as μ DBOs mature to hypertrophy.

tissue niches was yet to have an appreciable effect (supplementary figure 2). However, by day 7, striking differences in vascular morphogenesis with μ DBO maturity were observed (figure 5(A)(i)). The EC μ DBOs exhibited a pro-angiogenic phenotype that drives the invasion of small diameter vessels towards the μ DBOs. In contrast, the more differentiated MC μ DBOs exhibit an anti-angiogenic phenotype that inhibits vascular invasion in the area surrounding the μ DBO. Additionally, the vessels around MC μ DBOs were of larger diameter than with EC μ DBOs. As the μ DBOs mature to hypertrophy (HC), a morphologically different vasculature again surrounds the μ DBOs, with higher vascular coverage in the bulk gel. In an attempt to determine if paracrine factors secreted by the μ DBOs were responsible for changes in vascular formation, HUVEC only MPS devices were cultured in μ DBO conditioned media for seven days. Interestingly, similar vascular morphologies were observed in HUVEC only MPS devices fed with μ DBOs conditioned media (see supplementary figure 2), thus the observed differences in vascular morphology are at least partially attributable to

paracrine mechanisms. Perfusion of the formed vasculature shows that chondrogenic differentiation of the μ DBO impacts network development and function, as the vasculature surrounding these μ DBOs was unperfusable (figure 5(A)(ii)). However further μ DBO maturation to hypertrophy correlates with a switch to a more pro-angiogenic phenotype, as evident by the development of patent and perfusable vasculature.

Quantification of developing vascular networks confirmed the suppression of vascularisation around MC μ DBOs (figure 5(B)). Area vascularised, branch density, and junction density were significantly reduced in the area directly around the MC μ DBOs compared to vasculature in other regions of the same hydrogel. Even in regions of the gel distant to the μ DBO, the vasculature morphology was strongly dependent on phenotypic maturation, with markedly different morphologies depending on the μ DBO maturity. Less branched, thicker vessels were observed in the presence of hypertrophic μ DBOs. In addition, while μ DBOs dramatically influenced vascular architecture, the presence of ECs did not appear



to alter the morphology of the μ DBOs histologically (see supplementary figure 3).

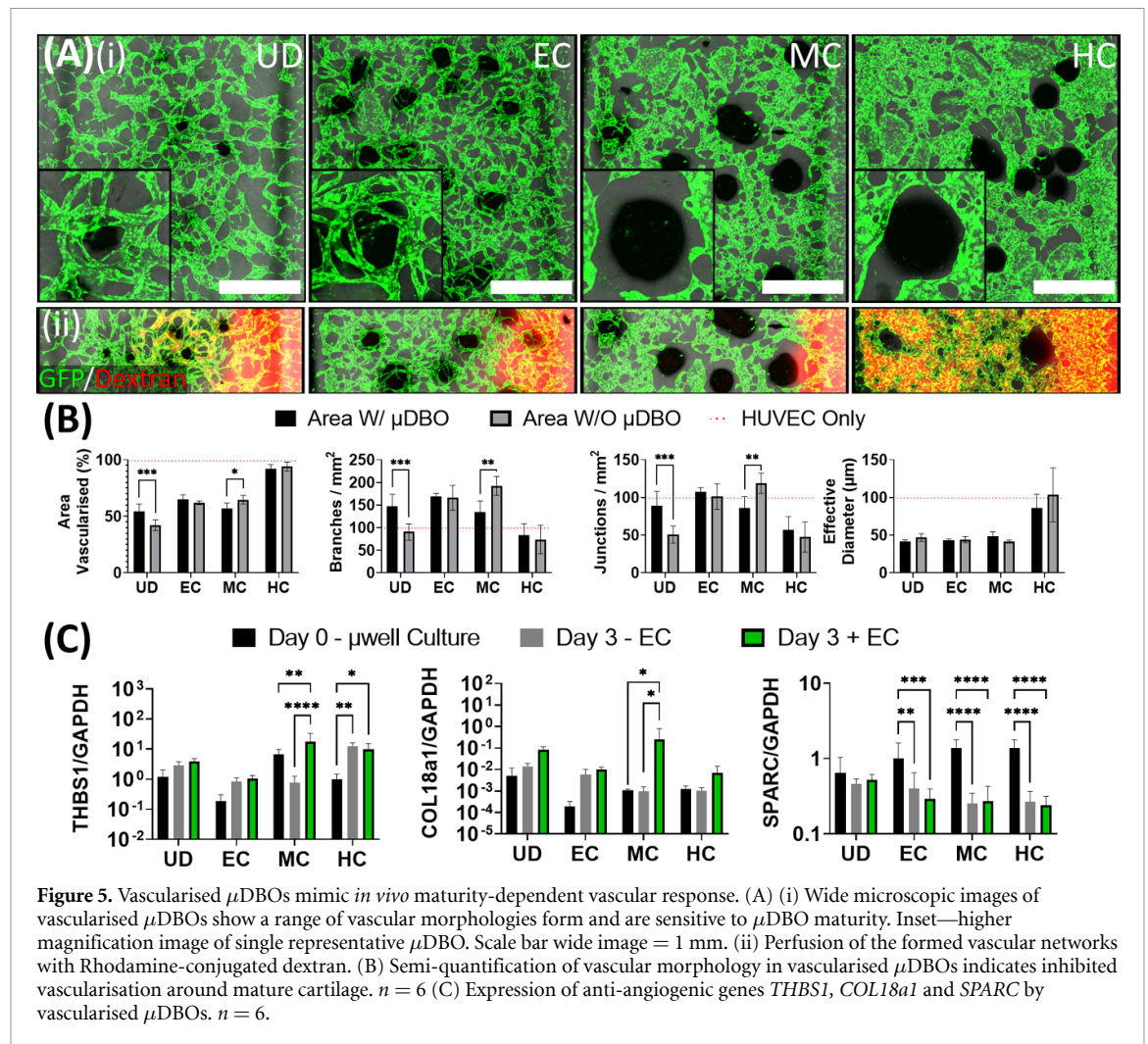
To investigate the mechanism by which μ DBOs exert their changing pro or anti-angiogenic effects, the expression of three anti-angiogenic genes was assessed; thrombospondin-1 (*THBS1*), Collagen type 18 (*COL18a1*) and Secreted Protein Acidic and Cysteine Rich (SPARC)/OSTEONECTIN (*SPARC*) (figure 5(C)). These genes were quantified before MPS culture (μ well culture), and after three days of MPS culture in the absence (–EC) and presence (+EC) of HUVECs. The expression of *THBS1* and *COL18a1* were both significantly upregulated in MC μ DBOs in the presence of ECs, correlating with the inhibition of vascularisation observed morphologically. In contrast, *SPARC* was downregulated in all differentiated spheroids in both vascularised and unvascularised conditions.

3.4. Vascularisation enhances the expression of the pluripotent factors SOX2 and OCT4 in DBOs

We next sought to examine whether this MPS could capture some of the key events observed during EO *in vivo*; the induction of pluripotency genes in chondrocytes with vascular invasion, and their subsequent trans-differentiation into osteoblasts. For this, gene expression in unvascularised μ DBOs (–ECs), vascularised (+EC), and μ DBOs before MPS seeding

(Day 0— μ well culture) were quantified using quantitative Reverse Transcription - Polymerase Chain Reaction (qRT-PCR). Interestingly, MPS culture (Day 3 \pm EC) generally increased the expression, though non-significantly, of pluripotency genes in all μ DBOs compared to day 0 μ well culture (figure 6(A)), indicating a possible effect of the angiogenic factors in the medium. However, the specific presence of vasculature significantly increased the expression of the pluripotency associated genes *SOX2*, and *OCT4* in MC DBOs, having no effect on the expression of these genes in UC, EC or HC μ DBOs. This indicates specific endothelial cell driven induction of pluripotency in the MC μ DBOs.

Next, the extent to which μ DBO vascularisation accelerated hypertrophy and progression towards an osteogenic phenotype was examined. Hypertrophic/osteogenic genes *RUNX2*, *MMP13*, and *COL10a1* were quantified after three and seven days in unvascularised and vascularised μ DBOs (figure 6(B)). At day 3, the presence of vasculature alone lead to a reduction in *RUNX2* expression in HC DBOs, but otherwise had little effect on hypertrophic/osteogenic gene expression. After seven days, the presence of the vasculature enhanced the expression of *MMP-13* in the EC DBOs, but had no effect on *RUNX2* or *COL10a1* expression. Gene expression was largely unaffected by vascularisation in



MC μ DBOs. Finally, in HC μ DBOs, the presence of vasculature again reduced the expression of *RUNX2*, but has no effect on *MMP-13* or *COL10a1* expression. Taken together, these results suggest vascularisation induces upregulation of hypertrophic genes, specifically *MMP-13*, in EC μ DBOs, but not in MC or HC μ DBOs for the relatively short culture periods assessed in this study (three or seven days).

4. Discussion

Transition of a cartilage template to bone during endochondral ossification is essential in bone development and regeneration, yet it is still poorly understood. The cartilage template matures over time during EO, initially suppressing but later promoting vascularisation of the developing bone template [35–37]. The change in cross-talk between these two tissue niches ensures proper bone development, and, in a therapeutic context, also dictates the potential of a cartilage template to effectively develop into bone tissue [10]. Currently, *in vitro* model systems to model and further understand this process are lacking [38]. Until advanced *in vitro* bone models have been developed and validated, the bone research

community will continue to rely on animal models that are under ethical scrutiny [39], can be prohibitively expensive, and do not adequately predict efficacy when translating bone therapies to humans [40]. In light of this problem, this study describes the design and development of an *in vitro* model of human EO consisting of DBOs and their interaction with invading vasculature. This MPS system is validated by demonstrating its potential to recapitulate key events observed during EO.

Angiogenesis of the developing bone rudiment occurs as the cartilage template matures towards hypertrophy. Thus, to further understand the crosstalk between vasculature and developing bone as it matures, a range of DBOs representative of different stages of early bone development (EC, MC, HC) was required. To achieve this, a μ well culture system was used to generate microscale cartilage μ DBOs for seeding within an MPS platform. Consistent with the literature [41], it was demonstrated that these microscale DBOs accumulate a cartilaginous matrix, mineralise, and exhibit an upregulation of genes associated with hypertrophy. Interestingly, mineralisation in these hypertrophic μ DBOs occurred in the core of the spheroids, which we have previously

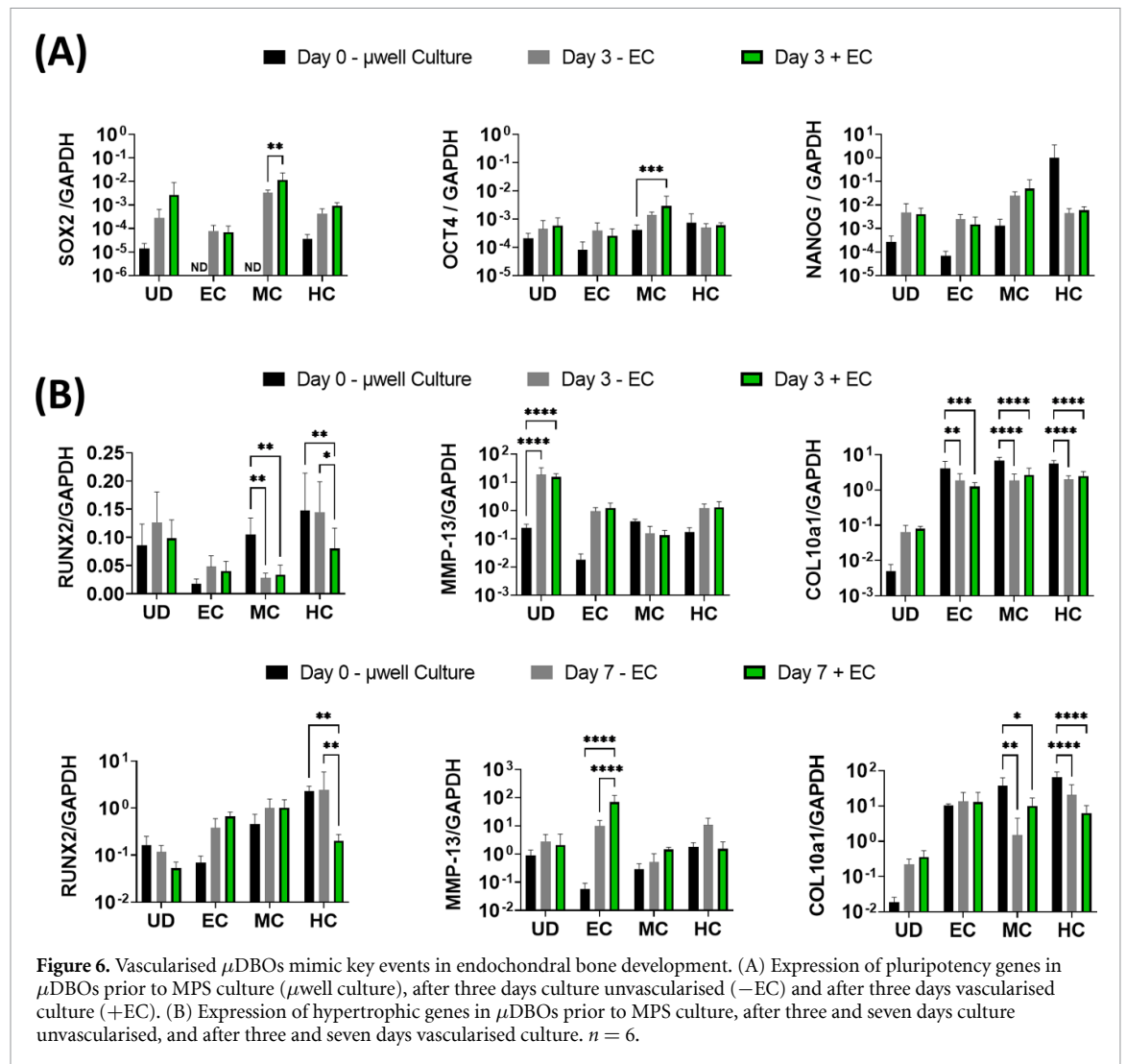


Figure 6. Vascularised μ DBOs mimic key events in endochondral bone development. (A) Expression of pluripotency genes in μ DBOs prior to MPS culture (μ well culture), after three days culture unvascularised ($-EC$) and after three days vascularised culture ($+EC$). (B) Expression of hypertrophic genes in μ DBOs prior to MPS culture, after three and seven days culture unvascularised, and after three and seven days vascularised culture. $n = 6$.

observed [31]. However, mineralisation on the outer surface of hMSC spheroids has also been observed in similar experiments [10]. The localisation of mineralisation is likely to be influenced by how specific experiment setups and spheroid sizes influences the oxygen tension within the spheroid, which has been shown to be a strong modulator of hypertrophic mineralisation [42]. As we used a standard model for inducing MSC chondrogenesis, we focused our analysis on the expression of hypertrophic and endochondral markers. Chondrogenesis with time in culture was confirmed by sGAG accumulation and standard histology; for further characterisation of such organoids, the interested reader is referred to our other work where we used these for putative therapeutic applications [25, 31, 43]. By simply terminating μ well culture at specific stages, micro-scale DBOs (μ DBOs) with unique phenotypes representative of the different stages observed in early endochondral bone development can be fabricated. Once primed in μ well culture, μ DBOs can be vascularised by seeding with endothelial cells in a matrix that permits vascular formation. Vascular networks

form within 4–7 days, which is consistent with systems using similar cells and matrices [44–46]. The advantage of this approach is that vasculogenesis can proceed in the presence of the μ DBOs, and the two tissues can be subsequently separated and analysed.

This model was able to recreate key biological phenomena that have been observed *in vivo*. Firstly, stable cartilage is avascular, and inhibits angiogenesis through the expression of anti-angiogenic factors [47] such as thrombospondin-1 [48], collagen type 18 [49], and SPARC [50], among others. In the model, inhibition of vascular invasion was observed around MC organoids, which correlated with an upregulation of THBS1. THBS1 exerts its antiangiogenic properties by three different mechanisms: ligation of CD36 on ECs to induce apoptosis [51], binding with the VLDL receptor to induce cell cycle arrest [52], and direct binding and inhibition of vascular endothelial growth factor (VEGF) via the low density lipoprotein receptor-related protein-1 (LRP-1) [53]. Morphologically, no cellular debris indicative of apoptosis was observed in the model, thus cell cycle arrest or VEGF inhibition would be more

likely candidate antiangiogenic mechanisms, which could be deciphered by probing for downstream effectors of both mechanisms with Ki67 or an LRP-1 antagonist. *COL18a1* was also upregulated in MC μ DBOs in the presence of vasculature. Endostatin is a cleaved fragment of collagen XVIII (gene product of *COL18a1*) that has well documented anti-angiogenic properties and is being trialled for treatment of solid tumours [54]. *COL18a1* was found to be upregulated in both unvascularised and vascularised μ DBOs, with vascularised μ DBOs having significantly upregulated expression, which corresponded with decreased vascularisation. Collagen XVIII is strongly expressed in cartilage and fibrocartilage [49] but not much else is known about its biogenesis, or induction of its expression. Finally, a downregulation of *SPARC* was observed in all μ DBO groups, irrespective of the presence of vasculature. Downregulation of *SPARC* coincided with both increased vascularisation around EC μ DBOs and decreased vascularisation around MC μ DBOs. The effects of *SPARC* are complex, as it has been demonstrated to have both angiogenic and anti-angiogenic effects [55]. In this case, *SPARC* could potentially be regulated by another protein that modulates its activity post-transcriptionally, such as TGF- β activation [56], where it is the variance in this factor that induces the variance in vascular phenotypes. Further studies would be required to test such hypotheses. Nevertheless, this model can successfully replicate the complex interaction between cartilage templates and invading vasculature during EO.

The MPS model was also able to recapitulate the vasculature-induced induction of pluripotency associated genes in hypertrophic chondrocytes, a phenomena observed during EO in fracture healing [1, 57, 58]. There was a general trend of increased *SOX2* expression in all μ DBOs in MPS culture relative to μ well culture. However, a significant increase in *SOX2* expression was evident in MC μ DBOs in the presence of vasculature. This correlates with vasculature induced *SOX2* expression observed in EO bone formation [1]. Thus, the model recreates vasculature induced expression of pluripotency genes *in vitro* and warrants exploration of canonical angiogenic growth factors as possible mediators of this induction. Similarly, there was a general trend of increased *OCT4* expression in μ DBOs cultured in MPS devices compared to μ well culture, with a significant upregulation in MC μ DBOs when co-cultured with vasculature. This finding on the chip agrees with the increased *OCT4* expression observed in chondrocytes undergoing EO mediated bone formation [1].

In the context of hypertrophy, the presence of vasculature had little effect on the expression of hypertrophic/osteogenic genes across all μ DBOs at day 3 post seeding in MPS devices. The exception to this

was in HC, where vasculature actually downregulated *RUNX2* expression. IGF-1, which is an essential component of the medium used in these experiments, has been used to promote stable cartilage formation and inhibits the expression of *RUNX2* and *MMP-13* [59], which may partially account for this particular observation. At day 7, vasculature again generally had little effect on osteogenic/hypertrophic gene expression, with *MMP-13* upregulation in EC μ DBOs the notable exception. This observation was amongst a general increasing trend in hypertrophic gene expression observed from day 3 to day 7 in all μ DBOs. It has been shown that angiogenic factors, such as VEGF, direct MSCs toward an osteoblastic phenotype, possibly accounting for this observation [60].

Additional steps are required to facilitate further development and validate the EO MPS. Firstly, our data suggests that ECs contribute to induction of pluripotency in μ DBOs, particularly in MC μ DBOs. However, it is also clear that μ DBOs are perhaps more sensitive to the angiogenic milieu of the EGM-2MV media that contains a number of angiogenic growth factors. While the model still substantiates the canonical actions of endothelial cells in EO driven bone formation, it also suggests that secreted angiogenic factors may have a significant role to play. In the context of model construction, HUVECs were used as they are a practical and well characterised primary human EC type for MPS applications. However ECs are a heterogeneous population that vary depending on their origin [61], and ECs specifically from bone have been shown to be sensitive to key signalling molecules involved in EO, such as PTHrP, while those from other tissues have not [62]. Nonetheless, the results described here indicate that the introduction of vasculature, and/or the angiogenic milieu, regulates the phenotype of human DBOs with MPS, enabling the developing of *in vitro* models of EO that mimic key phenomena observed *in vivo*.

5. Conclusions

This study details the development of an advanced *in vitro* model of EO. Specifically, we model the critical cross talk between developing bone and vasculature in EO that underpins the cartilage to bone transition. Our model mimics key events in endochondral bone development: the changing angiogenic profile of cartilage as hypertrophy proceeds as well as the vasculature induced expression of pluripotency associated genes in the cartilage template. Further development of these advanced *in vitro* systems could bring about a more complete understanding of EO, and has the potential to expedite the development of therapeutics for a range of skeletal conditions.

Data availability statement

All data that support the findings of this study are included within the article (and any supplementary files).

Acknowledgments

The authors gratefully acknowledge the financial support from Science Foundation Ireland (13/RC/2073).

ORCID iDs

Ian T Whelan  <https://orcid.org/0000-0002-9005-1439>

David A Hoey  <https://orcid.org/0000-0001-5898-0409>

Daniel J Kelly  <https://orcid.org/0000-0003-4091-0992>

References

- Hu D P, Ferro F, Yang F, Taylor A J, Chang W, Miclau T, Marcucio R S and Bahney C S 2017 Cartilage to bone transformation during fracture healing is coordinated by the invading vasculature and induction of the core pluripotency genes *Development* **144** 221–34
- Bahney C S, Hu D P, Miclau T and Marcucio R S 2015 The multifaceted role of the vasculature in endochondral fracture repair *Front. Endocrinol.* **6** 4
- Nandra R, Grover L and Porter K 2016 Fracture non-union epidemiology and treatment *Trauma* **18** 3–11
- Martini L 2004 *Encyclopedia of Endocrine Diseases* (Cambridge, MA: Elsevier Academic Press)
- Olstad K, Shea K G, Cannamela P C, Polousky J D, Ekman S, Ytrehus B and Carlson C S 2018 Juvenile osteochondritis dissecans of the knee is a result of failure of the blood supply to growth cartilage and osteochondrosis *Osteoarthr. Cartil.* **26** 1691–8
- Staines K, Pollard A S, McGonnell I M, Farquharson C and Pitsillides A A 2013 Cartilage to bone transitions in health and disease *J. Endocrinol.* **219** R1
- Freeman F E, Burdis R and Kelly D J 2021 Printing new bones: from print-and-implant devices to bioprinted bone organ precursors *Trends Mol. Med.* **27** 700–11
- Betz R R 2002 Limitations of autograft and allograft: new synthetic solutions *Orthopedics* **25** S561–70
- Sheehy E J, Mesallati T, Kelly L, Vinardell T, Buckley C T and Kelly D J 2015 Tissue engineering whole bones through endochondral ossification: regenerating the distal phalanx *BioRes. Open Access* **4** 229–41
- Scotti C, Tonnarelli B, Papadimitropoulos A, Scherberich A, Schaeren S, Schauerer A, Lopez-Rios J, Zeller R, Barbero A and Martin I 2010 Recapitulation of endochondral bone formation using human adult mesenchymal stem cells as a paradigm for developmental engineering *Proc. Natl Acad. Sci.* **107** 7251–6
- Daly A C, Pitacco P, Nulty J, Cunniffe G M and Kelly D J 2018 3D printed microchannel networks to direct vascularisation during endochondral bone repair *Biomaterials* **162** 34–46
- Daly A C, Cunniffe G M, Sathy B N, Jeon O, Alsberg E and Kelly D J 2016 3D bioprinting of developmentally inspired templates for whole bone organ engineering *Adv. Healthcare Mater.* **5** 2353–62
- Lanske B *et al* 1996 PTH/PTHrP receptor in early development and Indian hedgehog–regulated bone growth *Science* **273** 663–6
- Simpson A H and Murray I R 2015 Osteoporotic fracture models *Curr. Osteoporos. Rep.* **13** 9–15
- Emons J, Chagin A S, Säwendahl L, Karperien M and Wit J M 2011 Mechanisms of growth plate maturation and epiphyseal fusion *Horm. Res. Paediatr.* **75** 383–91
- Shukunami C, Shigeno C, Atsumi T, Ishizeki K, Suzuki F and Hiraki Y 1996 Chondrogenic differentiation of clonal mouse embryonic cell line ATDC5 *in vitro*: differentiation-dependent gene expression of parathyroid hormone (PTH)/PTH-related peptide receptor *J. Cell Biol.* **133** 457–68
- Newton P, Staines K A, Spevak L, Boskey A L, Teixeira C C, Macrae V E, Canfield A E and Farquharson C 2012 Chondrogenic ATDC5 cells: an optimised model for rapid and physiological matrix mineralisation *Int. J. Mol. Med.* **30** 1187–93
- Shukunami C, Ishizeki K, Atsumi T, Ohta Y, Suzuki F and Hiraki Y 1997 Cellular hypertrophy and calcification of embryonal carcinoma-derived chondrogenic cell line ATDC5 *in vitro* *J. Bone Miner. Res.* **12** 1174–88
- Mello M A and Tuan R S 1999 High density micromass cultures of embryonic limb bud mesenchymal cells: an *in vitro* model of endochondral skeletal development *Vitro Cell. Dev. Biol.* **35** 262–9
- Cheung J, Grant M E, Jones C, Hoyland J A, Freemont A J and Hillarby M C 2003 Apoptosis of terminal hypertrophic chondrocytes in an *in vitro* model of endochondral ossification *J. Pathol. A* **201** 496–503
- Hirao M, Tamai N, Tsumaki N, Yoshikawa H and Myoui A 2006 Oxygen tension regulates chondrocyte differentiation and function during endochondral ossification *J. Biol. Chem.* **281** 31079–92
- Grass G M and Sinko P J 2002 Physiologically-based pharmacokinetic simulation modelling *Adv. Drug. Deliv. Rev.* **54** 433–51
- Hann S Y, Cui H, Esworthy T, Zhou X, Lee S-J, Plesniak M W and Zhang L G 2021 Dual 3D printing for vascularized bone tissue regeneration *Acta Biomater.* **123** 263–74
- Chiesa I, De Maria C, Lapomarda A, Fortunato G M, Montemurro F, Di Gesù R, Tuan R S, Vozzi G and Gottardi R 2020 Endothelial cells support osteogenesis in an *in vitro* vascularized bone model developed by 3D bioprinting *Biofabrication* **12** 025013
- Nulty J, Burdis R and Kelly D J 2021 Biofabrication of prevascularised hypertrophic cartilage microtissues for bone tissue engineering *Front. Bioeng. Biotechnol.* **9** 661989
- Kim S, Lee H, Chung M and Jeon N L 2013 Engineering of functional, perfusable 3D microvascular networks on a chip *Lab Chip* **13** 1489–500
- Haase K and Kamm R D 2017 Advances in on-chip vascularization *Regen. Med.* **12** 285–302
- Jeon J S, Bersini S, Gilardi M, Dubini G, Charest J L, Moretti M and Kamm R D 2015 Human 3D vascularized organotypic microfluidic assays to study breast cancer cell extravasation *Proc. Natl Acad. Sci.* **112** 214–9
- Occhetta P, Mainardi A, Votta E, Vallmajo-Martin Q, Ehrbar M, Martin I, Barbero A and Rasponi M 2019 Hyperphysiological compression of articular cartilage induces an osteoarthritic phenotype in a cartilage-on-a-chip model *Nat. Biomed. Eng.* **3** 545
- Chou D B *et al* 2020 On-chip recapitulation of clinical bone marrow toxicities and patient-specific pathophysiology *Nat. Biomed. Eng.* **4** 1–13
- Burdis R, Chariyev-Prinz F, Browe D C, Freeman F E, Nulty J, McDonnell E E, Eichholz K F, Wang B, Brama P and Kelly D J 2022 Spatial patterning of phenotypically distinct microtissues to engineer osteochondral grafts for biological joint resurfacing *Biomaterials* **289** 121750
- Schindelin J *et al* 2012 Fiji: an open-source platform for biological-image analysis *Nat. Methods* **9** 676–82
- Arganda-Carreras I, Fernández-González R, Muñoz-Barrutia A and Ortiz-De-Solorzano C 2010 3D

- reconstruction of histological sections: application to mammary gland tissue *Microsc. Res. Tech.* **73** 1019–29
- [34] Pfeiffenberger M, Bartsch J, Hoff P, Ponomarev I, Barnewitz D, Thöne-Reineke C, Buttgereit F, Gaber T and Lang A 2019 Hypoxia and mesenchymal stromal cells as key drivers of initial fracture healing in an equine *in vitro* fracture hematoma model *PLoS One* **14** e0214276
- [35] Gerber H P, Vu T H, Ryan A M, Kowalski J, Werb Z and Ferrara N 1999 VEGF couples hypertrophic cartilage remodeling, ossification and angiogenesis during endochondral bone formation *Nat. Med.* **5** 623–8
- [36] Harper J and Klagsbrun M 1999 Cartilage to bone—angiogenesis leads the way *Nat. Med.* **5** 617–8
- [37] Pesesse L, Sanchez C, Delcour J-P, Bellahcène A, Baudouin C, Msika P and Henrotin Y 2013 Consequences of chondrocyte hypertrophy on osteoarthritic cartilage: potential effect on angiogenesis *Osteoarthr. Cartil.* **21** 1913–23
- [38] Schafrum Macedo A, Cezaretti Feitosa C, Yoití Kitamura Kawamoto F, Vinicius Tertuliano Marinho P, Dos Santos Dal-bó Í, Fiuza Monteiro B, Prado L, Bregadioli T, Antonio Covino Diamante G and Ricardo Auada Ferrigno C 2019 Animal modeling in bone research—should we follow the white rabbit? *Animal Models Exp. Med.* **2** 162–8
- [39] NC3Rs National Center for Replacement, Refinement, and Reduction of Animals in Research (available at: <https://www.nc3rs.org.uk/>) (Accessed 01 June 2022)
- [40] Klar R M 2018 The induction of bone formation: the translation enigma *Front. Bioeng. Biotechnol.* **6** 74
- [41] Johnstone B, Hering T M, Caplan A I, Goldberg V M and Yoo J U 1998 In vitro chondrogenesis of bone marrow-derived mesenchymal progenitor cells *Exp. Cell Res.* **238** 265–72
- [42] Sheehy E J, Buckley C T and Kelly D J 2012 Oxygen tension regulates the osteogenic, chondrogenic and endochondral phenotype of bone marrow derived mesenchymal stem cells *Biochem. Biophys. Res. Commun.* **417** 305–10
- [43] Burdis R, Kronemberger G S and Kelly D J 2022 Engineering high-quality cartilage microtissues using hydrocortisone functionalised microwells *Tissue Eng.* **28** 724–36
- [44] Watson S A *et al* 2022 Integrated role of human thymic stromal cells in hematopoietic stem cell extravasation *Bioeng. Transl. Med.* **8** e10454
- [45] Agrawal A, Shahreza S, Javanmardi Y, Szita N and Moendarbary E 2022 The tumour microenvironment modulates cancer cell intravasation *Organs-on-a-Chip* **4** 100024
- [46] Wan Z, Zhong A X, Zhang S, Pavlou G, Coughlin M F, Shelton S E, Nguyen H T, Lorch J H, Barbie D A and Kamm R D 2022 A robust method for perfusable microvascular network formation *in vitro Small Methods* **6** 2200143
- [47] Patra D and Sandell L J 2012 Antiangiogenic and anticancer molecules in cartilage *Expert Rev. Mol. Med.* **14** E10
- [48] Bornstein P 2009 Thrombospondins function as regulators of angiogenesis *J. Cell Commun. Signal.* **3** 189–200
- [49] Pufe T, Petersen W J, Miosge N, Goldring M B, Mentlein R, Varoga D J and Tillmann B N 2004 Endostatin/collagen XVIII—an inhibitor of angiogenesis—is expressed in cartilage and fibrocartilage *Matrix Biol.* **23** 267–76
- [50] Chandrasekhar S, Harvey A K, Johnson M G and Becker G W 1994 Osteonectin/SPARC is a product of articular chondrocytes/cartilage and is regulated by cytokines and growth factors *Biochim. Biophys. Acta—Mol. Cell Res.* **1221** 7–14
- [51] Volpert O 2000 Modulation of endothelial cell survival by an inhibitor of angiogenesis thrombospondin-1: a dynamic balance *Cancer Metastasis Rev.* **19** 87–92
- [52] Yamauchi M, Imajoh-Ohmi S and Shibuya M 2007 Novel antiangiogenic pathway of thrombospondin-1 mediated by suppression of the cell cycle *Cancer Sci.* **98** 1491–7
- [53] Greenaway J, Lawler J, Moorehead R, Bornstein P, LaMarre J and Petrik J 2007 Thrombospondin-1 inhibits VEGF levels in the ovary directly by binding and internalization via the low density lipoprotein receptor-related protein-1 (LRP-1) *J. Cell. Physiol.* **210** 807–18
- [54] Chen J *et al* 2018 A randomized Phase III trial of neoadjuvant recombinant human endostatin, docetaxel and epirubicin as first-line therapy for patients with breast cancer (CBCRT 01) *Int. J. Cancer* **142** 2130–8
- [55] Rivera L B, Bradshaw A D and Brekken R A 2011 The regulatory function of SPARC in vascular biology *Cell. Mol. Life Sci.* **68** 3165
- [56] Wrana J L, Overall C M and Sodek J 1991 Regulation of the expression of a secreted acidic protein rich in cysteine (SPARC) in human fibroblasts by transforming growth factor β : comparison of transcriptional and post-transcriptional control with fibronectin and type I collagen *Eur. J. Biochem.* **197** 519–28
- [57] Wong S A *et al* 2016 Trans differentiation of chondrocytes to osteoblasts during endochondral ossification in the healing mandible *FASEB J.* **30** 1039.11
- [58] Aghajanian P and Mohan S 2018 The art of building bone: emerging role of chondrocyte-to-osteoblast transdifferentiation in endochondral ossification *Bone Res.* **6** 1–9
- [59] Cucchiari M and Madry H 2014 Overexpression of human IGF-I via direct rAAV-mediated gene transfer improves the early repair of articular cartilage defects *in vivo Gene Ther.* **21** 811–9
- [60] Berendsen A D and Olsen B R 2015 Bone development *Bone* **80** 14–18
- [61] Harvey K, Welch Z, Kovala A T, Garcia J G N and English D 2002 Comparative analysis of *in vitro* angiogenic activities of endothelial cells of heterogeneous origin *Microvasc. Res.* **63** 316–26
- [62] Streen E A, Ornberg R, Curcio F, Sakaguchi K, Marx S, Aurbach G D and Brandi M L 1989 Cloned endothelial cells from fetal bovine bone *Proc. Natl Acad. Sci.* **86** 916–20